Ocean Engineering 254 (2022) 111331

Contents lists available at ScienceDirect

Ocean Engineering

journal homepage: www.elsevier.com/locate/oceaneng

Wake interactions of two horizontal axis tidal turbines in tandem

SeokKoo Kang [a,*], Youngkyu Kim [a], Jiyong Lee [b], Ali Khosronejad [c], Xiaolei Yang [d]

[a] Department of Civil and Environmental Engineering, Hanyang University, Seoul 04763, Republic of Korea
[b] St. Anthony Falls Laboratory, University of Minnesota, Minneapolis, MN 55455, USA
[c] Department of Civil Engineering, College of Engineering and Applied Sciences, Stony Brook University, Stony Brook, NY 11794, USA
[d] State Key Laboratory of Nonlinear Mechanics, Institute of Mechanics, Chinese Academy of Sciences, Beijing, 100190, China

ARTICLE INFO

Keywords:
Horizontal axis tidal turbine
Flow measurement
Turbine wake
Turbulence
Open-channel flow

ABSTRACT

The wake interactions between two horizontal axis model tidal turbines for two different spacings were investigated by flow measurements using acoustic Doppler velocimetry (ADV). The analysis of the velocity time-series data showed that a velocity sampling time period of at least 1000 integral time scales is required for the convergence of turbulence statistics in the wake of the turbines. The velocity measurement showed that a distinct three-layer (core, inner, and outer) structure was observed in the wake of a single turbine, whereas a simple wake pattern without such a structure was observed downstream of the two turbines. The comparison between the measurements for the different turbine spacings showed that the mean velocity fields, turbulent stress fields, velocity spectra plots, and integral length scales behind the second turbine were nearly independent of the turbine spacing. It was concluded that the increased turbulent momentum transfer across the wake boundary, mainly due to the wake meandering motion by the first turbine, overshadows the effect of the first turbine. This suggests that the ambient turbulence intensity induced by the upstream turbine could be a key factor for the wake characteristics within a tidal turbine array.

1. Introduction

Recently, tidal and ocean energy technologies have been developing faster than any other renewable energy technology because significant hydrokinetic energy sources in the oceans and coasts have remained untapped (Rourke et al., 2010; Lewis et al., 2015). According to Yuce and Muratoglu (2015), the globally available hydrokinetic energy from ocean waves and tidal currents is approximately 1550 TW h/year. Over the last decade, a number of commercial hydrokinetic turbines have been developed, such as the Verdant Power tidal turbine in the East River of New York City, USA (Gunawan et al., 2014); OpenHydro, HS1000, AR1000, and Voith tidal turbines at the European marine energy center (EMEC) tidal energy test facility (Zhou et al., 2014); and the SeaGen tidal turbine in Strangford Lough in Northern Ireland (Zhou et al., 2014). Several assessments on the recent advances in tidal and ocean energy technologies can be found in (Khan et al., 2009; Lago et al., 2010; Yuce and Muratoglu, 2015; Laws and Epps, 2016; Xie et al., 2020).

Horizontal axis tidal turbines have been studied extensively in tidal hydrokinetic energy research since the 2000s (Myers and Bahaj, 2007; Bahaj et al., 2007b,a; Batten et al., 2008; Maganga et al., 2010; Birjandi et al., 2013; Mycek et al., 2014b; Blackmore et al., 2016; Ouro et al., 2017). These turbines can efficiently harvest energy in rivers or tidal channels, where a predominant flow direction already exists. As is well known, multiple tidal turbines combined into an array can extract more power at a given site (Chen et al., 2017), and in this regard, horizontal axis tidal turbines can facilitate easy building of a tidal turbine array (or farm) comprising tens to hundreds of turbines.

Numerous attempts have been made to investigate the optimal tidal turbine array layouts by relying on analytical models, numerical simulations, or laboratory experiments. The analytic model studies (Stansby and Stallard, 2016; Brutto et al., 2016) usually employed optimization algorithms combined with simple wake models to find the optimal turbine layout. While these models have the capability of optimizing full-scale tidal farms with low computational costs, they cannot accurately account for the effects of currents and waves.

An alternative approach is to use a computational model that solves hydrodynamic equations. Some studies (Fallon et al., 2014; Chen et al., 2015) employed depth-averaged flow models to investigate the effect of turbine array configuration on the power output. These models, however, are inadequate for predicting complex three-dimensional turbulent flows within tidal turbine arrays owing to their two-dimensional flow assumptions. A more accurate and reliable approach at the expense of much higher computational cost is to use computational fluid dynamics (CFD) models, which solve the full three-dimensional

* Corresponding author.
E-mail address: kangsk78@hanyang.ac.kr (S. Kang).

https://doi.org/10.1016/j.oceaneng.2022.111331
Received 14 December 2021; Received in revised form 10 April 2022; Accepted 11 April 2022
Available online 28 April 2022

Navier–Stokes equations. Specifically, CFD models combined with turbine parameterization approaches, such as actuator disk (Yang et al., 2012) or line (Sørensen et al., 2015) approaches, have been used to simulate large wind farms (Yang et al., 2012; Castellani and Vignaroli, 2013; Yang and Sotiropoulos, 2018), individual tidal turbines (Batten et al., 2013; Sandoval et al., 2021), or small tidal farms containing several rows of turbines in an idealized setting (Apsley et al., 2018). A major limitation of using turbine parameterization approaches is its inability to account for the complex flow physics in the vicinity of tidal turbines, such as those associated with the tip vortices shed from turbine blades and hub vortex around the rotor axis (Kang et al., 2014). To circumvent this limitation, some CFD studies (Kang et al., 2012, 2014; Nuernberg and Tao, 2018b; Abuan and Howell, 2019; Zhu and Yan, 2021; Wang et al., 2021) attempted to simulate the rotation of tidal turbine rotors using fluid–structure interaction techniques. However, these approaches are inadequate for solving entire tidal turbine farm because of their enormous computational costs, which cannot be handled even with the computing power available today. At present, CFD modeling combined with turbine parameterization approaches is perhaps the most viable approach to simulate large tidal farms.

Laboratory experiments have been also used to investigate the flow field around tidal turbines. There are many studies on a single horizontal axis tidal turbine (Chamorro et al., 2013b; Neary et al., 2013; Chamorro et al., 2013a; Stallard et al., 2015; Mycek et al., 2014a; Morandi et al., 2016; Chen et al., 2017; Lee et al., 2020), but much less on tidal turbine arrays. Stallard et al. (2013), for instance, investigated the wake structures of several tidal turbine arrays consisting of up to ten, three-bladed horizontal axis turbines in a laboratory flume. They compared the velocity recovery in the wake regions of several different array configurations. Mycek et al. (2013) investigated the interaction between two tidal turbines with a spacing of $4D$, where D is the rotor diameter. They measured the axial velocity and turbulence intensity in the wake of the second turbine and showed that it is greatly affected by the upstream turbine. Mycek et al. (2014b) studied the flow field around two tidal turbines with spacings from $2D$ to $10D$ under different turbulence intensity conditions using laser Doppler velocimetry (LDV) measurements. They found that the turbulence intensity rather than the inter-device distance plays a significant role in the interaction effect between the two devices. Chawdhary et al. (2017) studied the wake characteristics of three horizontal axis turbines in the TriFrame configuration using flume experiments and turbine blade-resolving large-eddy simulation (LES). The TriFrame configuration consisted of three turbines mounted together at the apexes of a triangular frame with spanwise and streamwise spacings of $3D$ and $2D$, respectively. It was observed that the wake of the upstream turbine at the center of the TriFrame recovers faster than that of the other two owing to the Venturi effect. Nuernberg and Tao (2018a) conducted a flume experiment for a staggered tidal turbine array consisting of four horizontal axis turbines with various lateral and streamwise spacings using particle image velocimetry (PIV) measurements. The study showed that the lateral and longitudinal turbine spacing variations significantly affected the downstream flow field. Gaurier et al. (2020) investigated the interactions between three horizontal axis turbines with streamwise and spanwise spacings of $4D$ and $2D$, respectively, in a laboratory flume under different turbulence intensity conditions.

The aforementioned experimental studies are limited in several respects. First, only a few of them (Mycek et al., 2014b; Gaurier et al., 2020) reported detailed measurements of both velocity and turbulent (Reynolds) stress fields. Obtaining detailed velocity and Reynolds stress fields around (preferably realistic) tidal turbine arrays is critical for better understanding of the flow mechanisms within tidal turbine arrays. These data are also essential for the validation of CFD models. Second, the convergence of turbulence statistics has not been verified and discussed in most of the aforementioned studies. Flow around tidal turbines is inherently turbulent owing to the high Reynolds number, and for the measurement of turbulent flows, it is crucial to employ a sufficiently long velocity sampling time such that the turbulence statistics, including the Reynolds stresses that take longer to converge, can converge in time. Otherwise, the time-averaged turbulence statistics may be inaccurate or may not be reproducible by others. Third, flows in natural waterways tends to become fully developed as the boundary layers growing over the bed topography ultimately merge together. At a fully developed flow state, the time-averaged velocity and turbulence statistics no longer change in the streamwise direction. Further, the flow in the near-bed region is characterized by a steep velocity gradient and strong turbulence intensity. Although understanding the turbine wake interactions under realistic inflow conditions is critical to the optimal design of tidal turbine arrays, fully developed turbulent inflow conditions have rarely been considered in previous experiments. Owing to the aforementioned limitations and a lack of related research, the current understanding of the flow mechanisms within tidal arrays remains incomplete.

This study is motivated by the need to improve the understanding of the flow mechanisms within tidal arrays through detailed flow measurements. Specifically, the present study aims to investigate the turbine spacing effects on the mean and turbulent flow characteristics in the wake of two aligned tidal turbines. Turbine spacing is one of the most important factors influencing the performance of a tidal array, but their effects on the turbine wake interactions or turbine array efficiency are not yet well understood. To date, no consensus has yet been reached on the optimal turbine layout or spacing that provides the maximum array efficiency. Another motivation for this study is to secure reliable experimental data that can be used to validate CFD models. CFD results for tidal turbine array simulations performed up to now have rarely been validated using data from well controlled laboratory experiments, possibly due to the lack of such data. For this reason, it is not yet known, to what degree of accuracy, CFD models using turbine parameterization approaches can simulate the complex flows within tidal turbine arrays. To the authors' knowledge, measurements and comparisons of detailed velocity and turbulent stress fields in the wake of an aligned turbine array for different turbine spacings have not yet been performed.

The present study focuses on addressing the current knowledge gaps by carrying out detailed velocity measurements downstream of two model horizontal axis tidal turbines aligned with the flow direction. The model turbines are based on the three-bladed Gen4 turbine developed by Verdant Power for the Roosevelt Island Tidal Energy (RITE) project in the East River in New York (Kang et al., 2014). Two sets of experiments were carried out for the turbines with streamwise spacings of $5D$ and $7D$. These spacings were comparable to those ($4D$ and $7D$) used in mobile-bed flume experiments by Hill et al. (2016) for a model tidal turbine with the same rotor design. Velocity profile measurements were taken using acoustic Doppler velocimetry (ADV) for an axial distance of up to $10D$ at a total of sixteen axial locations. To ensure the time convergence of the flow statistics, the time-averaged flow statistics were compared for variable sampling windows sizes, and from which the minimum sampling period was proposed. Using the mean velocity and turbulence fields, the turbine spacing effects on the wake characteristics of the two aligned tidal turbines were investigated. Using the velocity time series data, the power spectral densities of the velocity fluctuations and integral length scales were also investigated. To the best of the authors' knowledge, this study is the first to present and compare detailed mean velocity and Reynolds stress measurements in the wake of two model tidal turbines with the verification of their statistical convergence.

2. Experimental set-up

Flume experiments were conducted in an open-channel flume at the department of Civil and Environmental Engineering at Hanyang University, Seoul, South Korea. The dimensions of the flume were of 18 m, 0.9 m, and 0.4 m in the streamwise, spanwise, and vertical

Table 1
Experimental conditions. g is the acceleration due to gravity.

Rotor diameter (D)	0.16 m
Mean water depth (H)	0.37 m
Hub height above the bed (z_{hub})	0.136 m
Bulk velocity (U_b)	0.19 m/s
Approach velocity at the hub height (U_0)	0.21 m/s
Blockage ratio	6.0%
Froude number ($Fr = U_b/\sqrt{gH}$)	0.10
Average water temperature	$22°C$
Reynolds number, Re_H ($= U_0 H/\nu$)	8.13×10^4
Reynolds number, Re_D ($= U_0 D/\nu$)	3.51×10^4
Tip speed ratio (λ)	5.10
Turbine spacing (s)	$5D$, $7D$
Incoming turbulence intensity	4.5%

directions, respectively. The sidewalls of the flume were made of glass and the bed was made of polyvinyl chloride.

Fig. 1 shows the photographs of the turbines and open-channel flume. Two turbines were installed at the center of the channel facing downstream in such a way that their rotor axes are aligned with the streamwise direction. Two different streamwise spacings (s), $s = 5D$ and $7D$, were considered. As illustrated in the figure, the turbine rotor diameter (D) is 0.16 m, which is approximately a 1:31 scale model of the Gen4 turbine rotor, and the hub height z_{hub} is 0.136 m. The model turbine consisted of three parts: the rotor, nacelle, and tower. Each part was manufactured using an Ultimaker-2 3D printer with polylactic acid plastic filament. Subsequently, the 3D-printed parts were assembled with a direct current (DC) motor connected to an external power source by an electrical wire. The angular speed of the turbine rotor was adjusted to a desired value by changing the current from the external power source to the DC motor, which yielded a specific tip speed ratio (TSR). A TSR is defined as the ratio of the tangential speed of the blade tip to the reference velocity upstream of the rotor. Both the first (upstream) and second (downstream) turbines operated at the same angular velocity, which yielded a TSR (λ) of 5.1, based on the mean flow speed at the hub height upstream of the first turbine. Although the turbine power outputs were not measured in this study, the power of a turbine with the same blade design but with a different rotor diameter ($D = 0.5$ m) was measured by Chamorro et al. (2013a). According to the power coefficient curve presented in that study, the maximum power coefficient (C_p) occurs at $\lambda = 5.8$, and C_p at $\lambda = 5.1$ is approximately 90% of the maximum value. The blockage ratio in the present experiment was approximately 6 %. Chamorro et al. (2013a) also used the same blockage ratio and reported negligible blockage effects. Nevertheless, it is still possible that the wake measurements were slightly affected by the blockage effect. Lee et al. (2020) performed laboratory experiments for the same single turbine under the same flow conditions as in the present study, which has been considered as the baseline case for the two experiments carried out in this study. The detailed experiment conditions are listed in Table 1.

The model turbine prototype is the Gen4 Verdant Power turbine, a three-bladed, horizontal axis turbine with a diameter of 5 m. It was developed with the aim of installing 1.05 MW arrays of thirty 35 kW turbines in the East Channel of the East River, New York City (see Kang et al., 2012; Gunawan et al., 2014, for more details). Currently, five turbines have been successfully deployed in the channel, and more turbines are planned to be installed in 10 TriFrame arrangements, i.e., sets of three turbines will be mounted on the apexes of a common triangular base. Because this specific turbine is one of the few currently operating hydrokinetic turbines, it has been studied extensively by researchers (Kang et al., 2012; Neary et al., 2013; Chamorro et al., 2013a; Kang et al., 2014; Hill et al., 2016; Chawdhary et al., 2017; Musa et al., 2018, 2019; Lee et al., 2020).

It is worth mentioning that the turbine rotor diameter ($D = 0.16$ m) used in this study is relatively small compared to the previous experiments (Chamorro et al., 2013a; Stallard et al., 2015; Chen et al., 2017; Mycek et al., 2014a,b; Nuernberg and Tao, 2018a; Gaurier et al., 2020; Ebdon et al., 2021), where D was 0.27 to 0.7 m. Larger turbines are less affected by scale effects and therefore may be more suitable for measuring turbine performance (torque and power). However, large devices can cause difficulties in obtaining fully developed turbulent inflow conditions in a laboratory channel of moderate length. To create a fully developed flow at a turbine location, the first turbine should be installed after the entrance length (L_e), which is defined as a distance from the channel inlet required to achieve fully developed turbulent flow. It is well known that L_e increases with depth, but depth should also increase with turbine diameter to maintain low blockage ratio. In our previous experiment for a single tidal turbine (Lee et al., 2020), the entrance length was approximately $20H$ (≈ 7.5 m). In the present study, the turbine diameter ($D = 0.16$ m) and depth ($H = 0.37$ m) were determined such that: (1) the first turbine is positioned behind the entrance length (≈ 7.5 m); (2) the turbine blockage ratio is less than 10%; and (3) at least $15H$ (≈ 5.5 m) remains downstream of the second turbine to take wake measurements without being affected by a tailgate at the end of the flume. Unless small-size turbines are used, it is very difficult to achieve a fully developed turbulent inflow in laboratory flume of limited length. For instance, Ebdon et al. (2021) performed wake measurements for a tidal turbine at $D = 0.5$ m and $H = 2$ m in an 18-m long flume. If the relation $L_e = 20H$ is used, the entrance length is estimated to be approximately 40 m, which exceeds the total length (18 m) of the flume.

Fig. 2 illustrates the turbine arrangement in the flume, the coordinate system, and the velocity measurement locations. Here, x and x' indicate the streamwise coordinates relative to the rotor planes of the first (T_1) and second (T_2) turbines, respectively. y indicates the spanwise coordinate from the rotor axis toward the left-side vertical wall when viewed from an upstream location. z and z' indicate the vertical coordinates relative to the channel bed and hub height, respectively.

The instantaneous velocities were measured in the xz plane passing through the center of the rotor using a Nortek Vectrino Profiler ADV at a sampling rate of 100 Hz for 480 s. A total of sixteen vertical measurement profiles were obtained for $-2 \le x/D \le 10$. Each profile consisted of thirty measurement points spaced at $0.0625D$ (=1 cm). The velocities were measured continuously for 480 s at each measurement point without taking into account the instantaneous angular position of the rotor blades. That is, the measurement timing was not synchronized with the rotation of the blades.

3. Results and discussions

In this section, the mean velocity field, turbulent stress field, power spectral densities of velocity fluctuations, and integral length scales are presented and analyzed. In the remainder of this study, u, v, and w indicate the instantaneous velocity components in the x, y, and z directions, respectively. $\langle q \rangle$ indicates the time-averaging operation for a variable q, that is, $\langle q \rangle = \sum_{i=1}^{N} q_i/N$, where N is the total number of velocity samples. q' denotes the fluctuating component of q, that is, $q' = q - \langle q \rangle$. The turbulence kinetic energy (TKE) is defined as $k = 0.5\left(\langle u'u' \rangle + \langle v'v' \rangle + \langle w'w' \rangle\right)$.

3.1. Convergence of flow statistics

The flow in the wake of a horizontal axis tidal turbine is characterized by the turbulent structures involving a wide range of scales, varying from fine-scale turbulence in the vicinity of the rotor blades to large-scale flow motions away from the turbine. To accurately capture all the important flow scales, especially those of low-frequency and large-scale motions, the sampling time should be sufficiently long. The

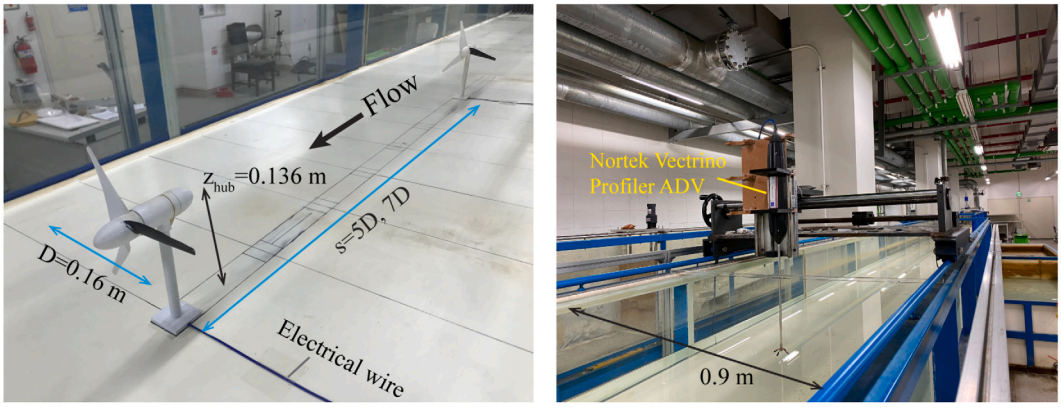

Fig. 1. Photographs of the turbines and the laboratory flume.

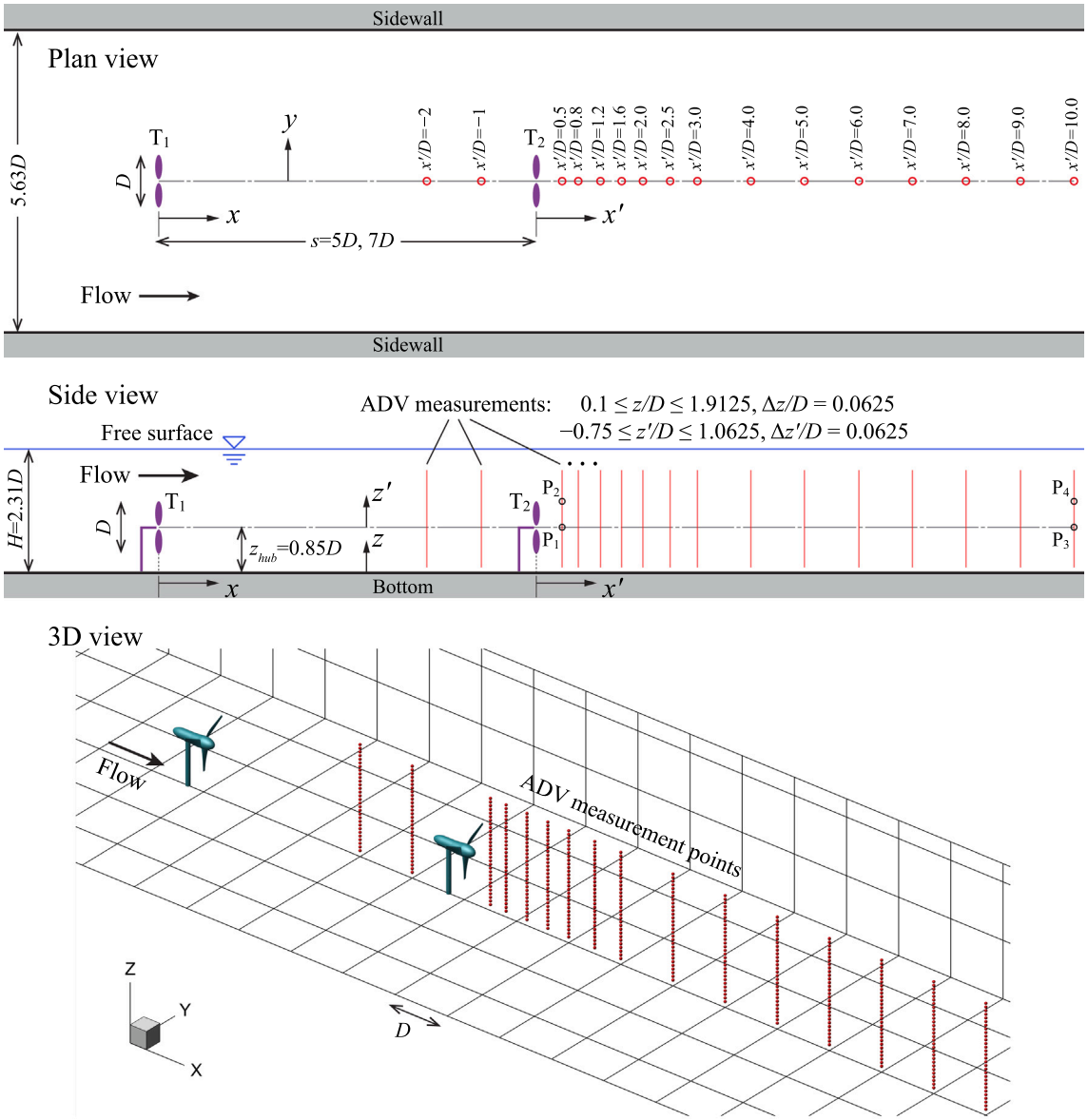

Fig. 2. Coordinate system and ADV measurement locations in the flume. T_1: upstream turbine, T_2: downstream turbine. The (x', z') coordinates of the points P_1, P_2, P_3, and P_4 are $(0.5D, 0)$, $(0.5D, 0.5D)$, $(10D, 0)$, and $(10D, 0.5D)$, respectively.

minimum time required to obtain accurate flow statistics for the tidal turbine experiments is yet to be reported.

To assess the effect of the sampling time period on the flow statistics, the turbulence statistics for the $s = 5D$ case at four representative

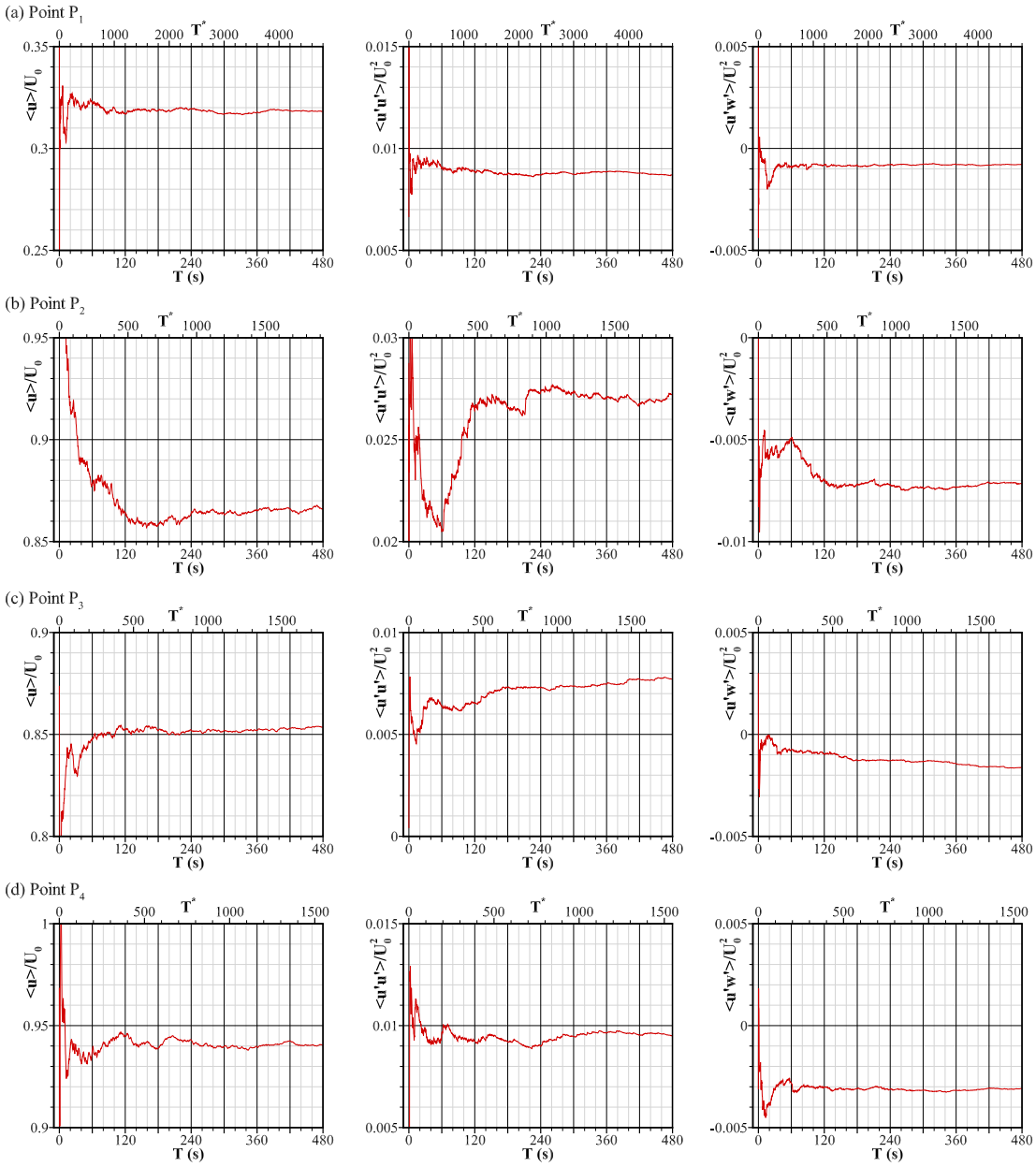

Fig. 3. Convergence of the turbulence statistics for the $s = 5D$ case with varying sampling time windows at the points (a) P_1, (b) P_2, (c) P_3, and (d) P_4, as shown in Fig. 2.

locations, P_1 to P_4 as shown in Fig. 2, were calculated for variable sampling window sizes (T) up to 480 s. Of all the measurement points, P_1 and P_2 were the closest to and P_3 and P_4 were the farthest from the second turbine (T_2).

In Fig. 3, the variations in the flow statistics $\langle u \rangle$, $\langle u'u' \rangle$, and $\langle u'w' \rangle$ are plotted for a variable sampling time T. A dimensionless time window size T^* is shown on the upper horizontal axis, which is defined as $T^* = T/I_T$. I_T is an integral time scale defined in Eq. (1) in Section 3.4. The integral time scales for points P_1 to P_4 are 0.10 s, 0.25 s, 0.27 s, and 0.31 s, respectively. At point P_1, the statistical convergences of $\langle u \rangle$, $\langle u'u' \rangle$, and $\langle u'w' \rangle$ occur at approximately $T = 100\ s$. At points P_2 to P_4, the convergence of $\langle u \rangle$ occurs approximately at $T = 240$ s, whereas those of $\langle u'u' \rangle$ and $\langle u'w' \rangle$ occur at approximately $T = 300$ s. As witnessed above, the sampling time required for the convergence varies from 100 to 240 s at points P_1 to P_4. However, it is worth pointing out that the dimensionless sampling window size required for the convergence is approximately $T^* = 1000$ regardless of the location. This is because the minimum required sampling time is associated with an integral scale. The aforementioned results show that the physical time required for the convergence can differ significantly at different locations; however, the dimensionless time in terms of the local integral time scale is constant at approximately 1000. Based on these results, a minimum sampling time of at least 1000 integral time scales is proposed for the convergence of both the first- and second-order flow statistics in the wake of the two turbines. This number may also be applicable to a single turbine experiment, as the integral scales in the far wakes of the single turbine and the two turbines are nearly the same, as demonstrated in Section 3.4. The sampling time of 480 s employed in this study corresponds to approximately 1500 to 4800 integral time scales at points P_1 to P_4, significantly greater than the recommended number of 1000.

It is worth noting the sampling time employed in previous experimental studies on horizontal axis turbines. Unfortunately, only a few studies have reported the integral scales. For instance, Gaurier et al. (2020) reported that for three tidal turbines ($D = 0.7$ m and $U_0 = 0.79$ m/s) in a triangular arrangement the integral length scales for low

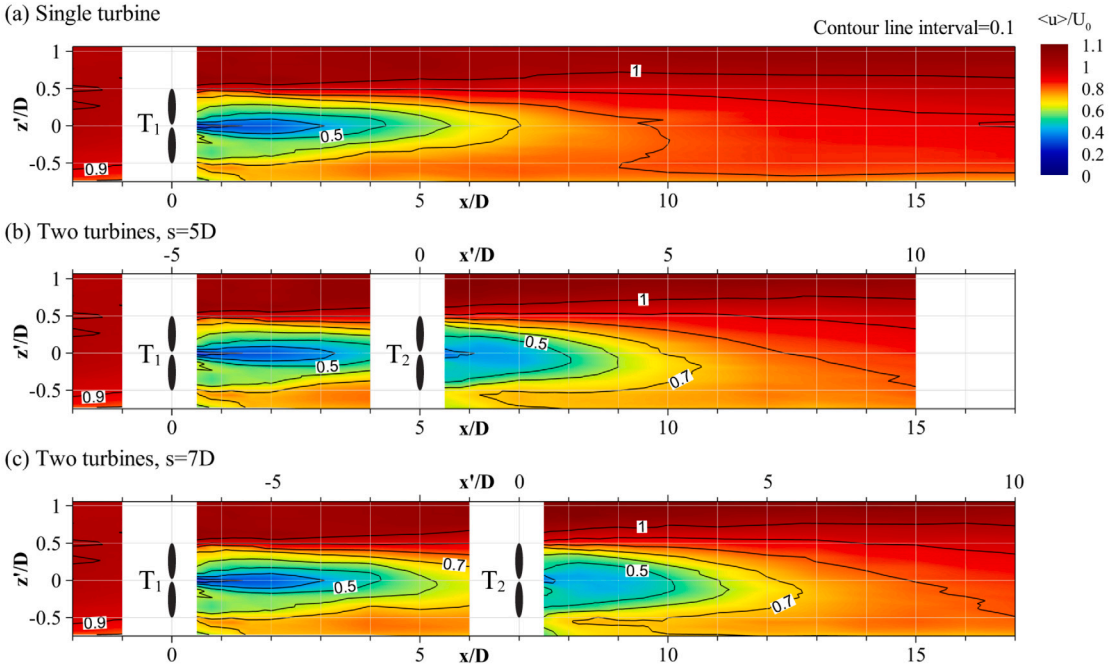

Fig. 4. Contours of the time-averaged axial velocity. (a) single turbine, (b) two turbines with $s = 5D$, (c) two turbines with $s = 7D$.

and high turbulence intensity conditions were between 0.6 and 0.9 m. Using the Taylor's frozen turbulence hypothesis, the corresponding integral time scales of the two cases can be estimated to be between $\frac{0.6\text{ m}}{0.79\text{ m/s}} \approx 0.76$ s and $\frac{0.9\text{ m}}{0.79\text{ m/s}} \approx 1.14$ s. Additionally, the velocity was measured using a LDV for 180 s, which corresponds to approximately 160–240 integral time scales. Chamorro et al. (2013a) measured the flow past a single tidal turbine ($D = 0.5$ m and $U_0 = 0.4$ m/s) using an ADV with the sampling duration of 300 s. The integral length scale was reported to be approximately $0.35D$ (≈0.175 m). Similar to the aforementioned case, the integral time scale is estimated to be $\frac{0.175\text{ m}}{0.4\text{ m/s}} \approx 0.44$ s. Thus, 300 s corresponds to approximately 680 integral time scales. The previous rough calculations show that the sampling times in both studies were less than 1000 integral time scales, which, based on the authors' suggestion, could be insufficient to obtain fully converged turbulence statistics in the wake.

3.2. Mean flow and turbulence fields

The contours of the mean velocity and turbulence stress fields are shown in Figs. 4–7. The results of a single turbine experiment under the same flow conditions (Lee et al., 2020) are shown in Figs. 4(a)–7(a) for comparison purposes. Additionally, the vertical profiles of the mean streamwise velocity for the measurement sections in the wake of the second turbine are displayed in Fig. 8. As mentioned in Section 2, the velocity measurement was performed for the region $-2 \le x'/D \le 10$ in the present study. The flow measurement was not taken in $x'/D < -2$, as the flow in this region was not affected by the presence of the second turbine. Hence, the velocity measurements from the single turbine experiment for the region $x'/D < -2$ were stitched together with the measurements of this study and plotted in Figs. 4(b)–7(b) and 4(c)–7(c).

First, the wake patterns of T_2 were investigated. Kang et al. (2012) used numerical simulations to show that the instantaneous wake structure of the prototype tidal turbine with the same rotor design as the proposed model consisted of three distinct regions: (1) the outer layer, where the blade tip vortices rotate around the wake in the same direction as the blades; (2) the inner layer, where the wake counter-rotates to the outer layer; and (3) the core layer, where the axial velocity is very low and the flow co-rotates with respect to the outer layer. Figs. 4(a)–7(a) show that these three-layer structures are also visible in the time-averaged wake of T_1. Specifically, a thin elongated region with low axial velocity and high TKE around the rotor axis marks the core layer. The near-wake regions between the rotor axis and the blade tips with a large rotational velocity show the inner layer. An exceptionally thin layer with a high TKE and $\langle u'w' \rangle$ Reynolds stress at the top blade tip show the outer layer. These high turbulence levels are associated with the velocity fluctuations induced by the blade tip vortices. At the bottom tip, however, the thin layer is not observed owing to the wake effect of the turbine supporting structure upstream of the rotor (Lee et al., 2020). An additional notable flow feature found in the wake of T_1 is an abrupt increase in the TKE and $\langle u'w' \rangle$ Reynolds stress at $x/D \approx 4$, which has been shown to be associated with the onset of wake meandering (Kang et al., 2014). Wake meandering, also observed for the wind turbines, is known to cause the entire wake body to move along the transversal and vertical directions at low frequencies.

In comparison with T_1, the wake patterns of T_2 did not clearly show the three-layer structure for both spacings. Figs. 6(b), 6(c), 7(c), and 7(d) show that the shear layers emanating from the top and bottom blade tips are much thicker and spread at a much faster rate toward the rotor axis. Moreover, Figs. 5(b) and 5(c) show that the rotational velocity is considerably lower compared with the single turbine case and, that becomes virtually negligible at $x'/D = 1$. Another important finding from the comparisons of the flow field contours between the $s = 5D$ and $s = 7D$ cases is that the wake patterns of T_2 are exceedingly similar to each other (also shown in Fig. 8), despite the different approach velocity distributions directly upstream ($x'/D = -1$) of T_2 as deduced from comparing Figs. 4(b) and 4(c). This suggests that the wake patterns of the second turbine are independent of the streamwise turbine spacing.

It is noteworthy that the simple wake patterns behind T_2 appear quite similar to those predicted by the flow models using the actuator disk models (Yang et al., 2012; Castellani and Vignaroli, 2013; Yang and Sotiropoulos, 2018). These models treat a turbine rotor as a porous disk absorbing the fluid momentum while disregarding the rotational flow effects. The flow field predicted by these models is characterized by the shear layers spreading from the edges to the center of the disk. The reason for the similarity is possibly due to the negligible rotational velocity in the wake of T_2, which is the underlying assumption behind

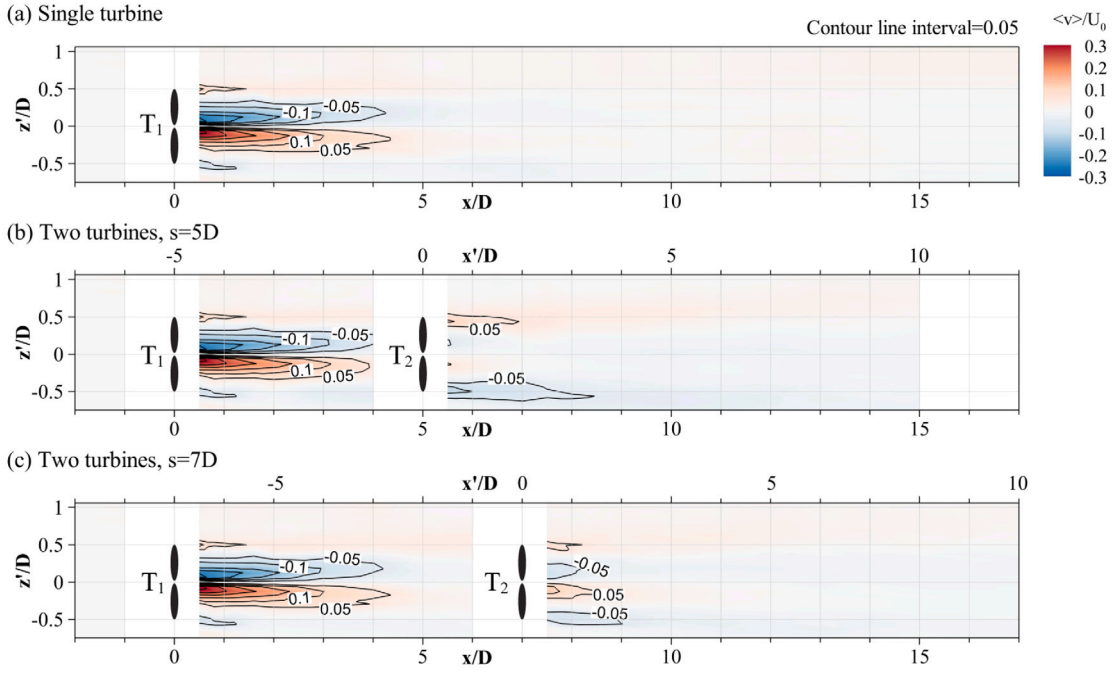

Fig. 5. Contours of the time-averaged transverse (y) velocity. (a) single turbine, (b) two turbines with $s = 5D$, (c) two turbines with $s = 7D$.

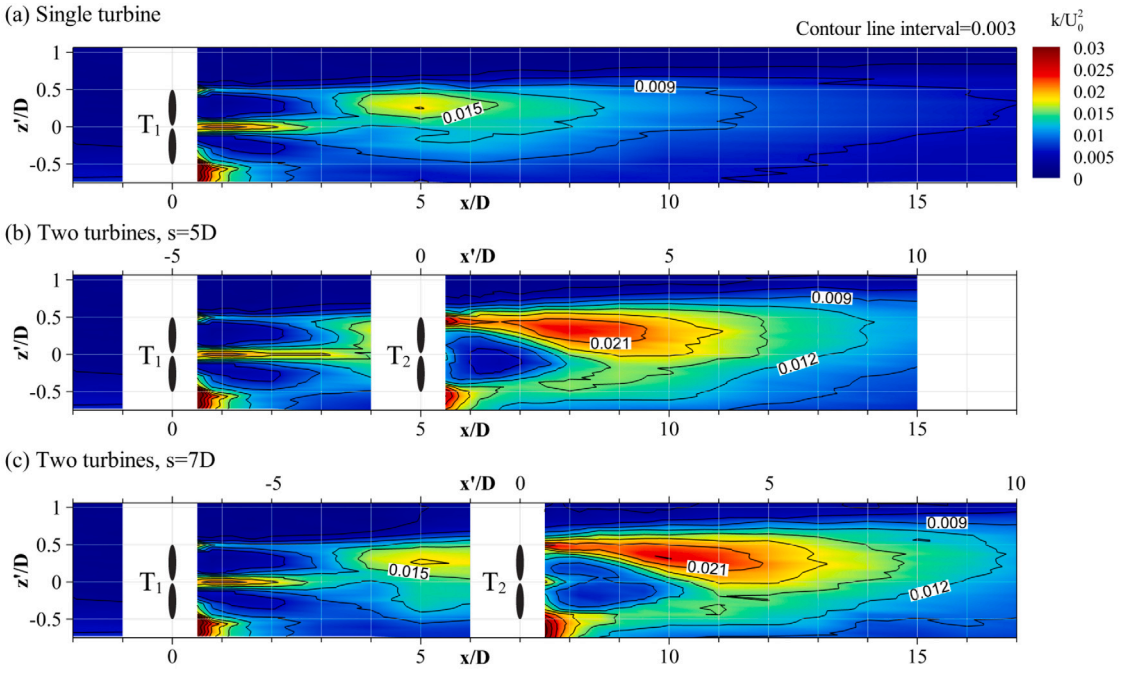

Fig. 6. Contours of the TKE. (a) single turbine, (b) two turbines with $s = 5D$, (c) two turbines with $s = 7D$.

the actuator disk model. It can be postulated that the third or fourth turbines behind T_2 that are placed at locations under similar turbulence intensity may produce similar wake patterns. This implies that the flow in a large tidal farm can be easily modeled using a turbine parameterization approach, instead of the costly turbine geometry resolving approach (Kang et al., 2012, 2014). A similar conclusion was derived by Aubrun et al. (2013) through wind tunnel experiments for a model wind turbine with a realistic rotor design and a porous disk generating a similar velocity deficit. They showed that under a high turbulence intensity condition, the rotational momentum generated by the rotor blades and the tip vortex signatures were not detectable at the downstream locations farther than three rotor diameters from the turbine, and the wake of a realistic turbine could be reproduced accurately using a porous disk.

In Fig. 9, the axial profiles of the mean velocity deficit, $1 - \langle u \rangle / U_0$, and the TKE at the hub height ($z' = 0$) are compared between the cases of $s = 5D$ and $7D$. The results are plotted on the x coordinate in Figs. 9(a) and 9(c), and on the x' coordinate in Figs. 9(b) and 9(d). The velocity deficit profiles plotted on the x' coordinates for the two cases are remarkably similar throughout the wake region. In addition, the TKE profiles show excellent agreement, particularly for $x'/D > 2$. This result combined with the comparisons of the flow fields shown in Figs. 4–7, confirm that the wake patterns of T_2 are nearly

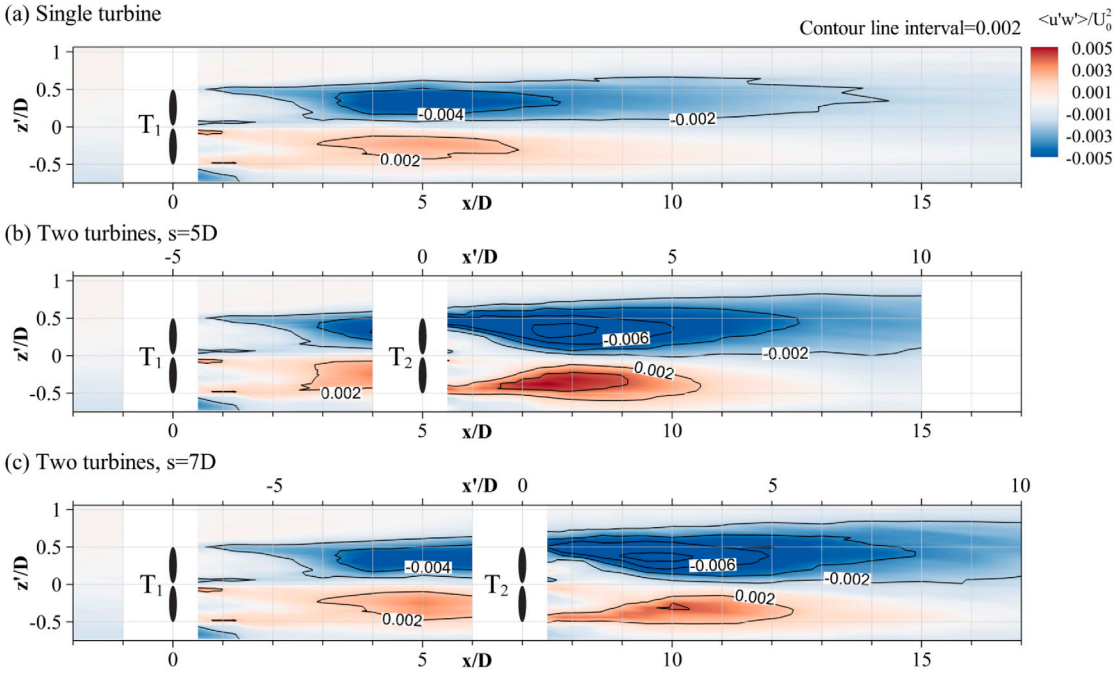

Fig. 7. Contours of $\langle u'w' \rangle$. (a) single turbine, (b) two turbines with $s = 5D$, (c) two turbines with $s = 7D$.

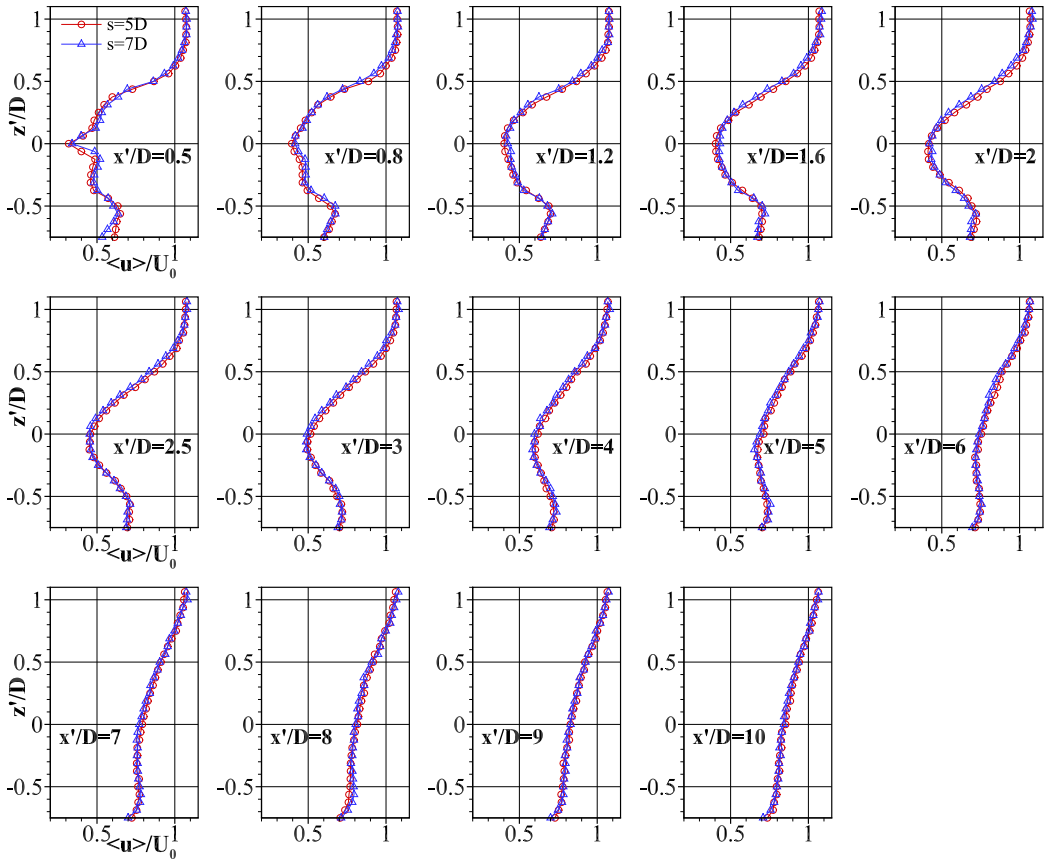

Fig. 8. Vertical profiles of the mean streamwise velocity in the wake of the second turbine.

independent of the turbine spacing. This is unexpected, as the approach flow velocities at $x'/D = -1$ and -2 differ by approximately 20%.

The aforementioned results show that the wake patterns of T_2 between the cases for $s = 5D$ and $7D$ are remarkably similar, both quantitatively and qualitatively. In this study, it has been hypothesized that this similarity is associated with the high turbulence levels around T_2, which is due to the wake meandering induced by T_1. Fig. 6(a) shows that the dimensionless TKE of the single turbine case at the locations of T_2 ($5 \leq x/D \leq 7$) varied from 0.012 to 0.015, which is significantly greater than that upstream of T_1. The high incoming

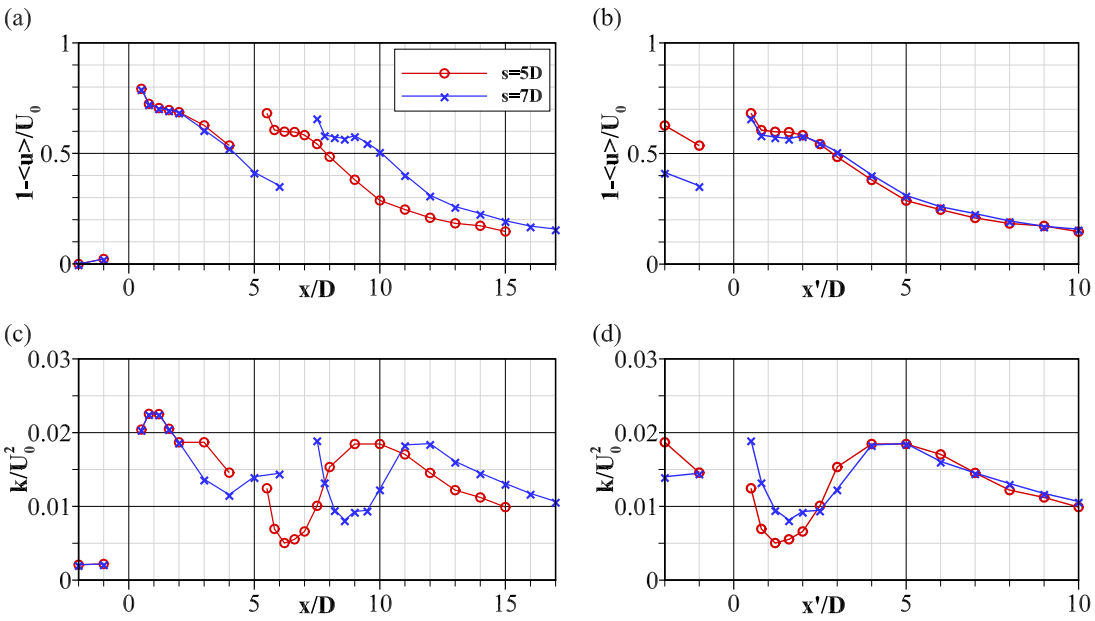

Fig. 9. Axial profiles of the mean velocity deficit and the TKE at the hub height. (a) velocity deficit on the x coordinate. (b) velocity deficit on the x' coordinate. (c) TKE on the x coordinate. (d) TKE on the x' coordinate.

turbulence levels around T_2 combined with the turbulence generated by the rotor blades are expected to further increase the turbulent levels in the wake of T_2. This is confirmed by the dimensionless TKE levels in the wake of T_2, which increased to approximately 0.02. The role of the increased turbulence levels in the wake is to transfer the mean flow energy from the ambient flow to the wake region, which is used for the momentum recovery in the wake. The similar wake patterns observed for the two different spacings, despite the different approach velocities, are presumably due to the turbulent momentum transfer between the wake and the ambient flow, which overshadows the effect of the approach velocity.

3.3. Power spectral density

In Fig. 10, the power spectral density of the vertical velocity fluctuation E_{ww} and the pre-multiplied spectra fE_{ww} are plotted, where f is the frequency.

The spectra of the approach flow at $x'/D = -1$, which is directly upstream of T_2, exhibit a spectral peak at $f \approx 0.35$ Hz. This frequency corresponds to the Strouhal number of $St \approx 0.27$, where $St = fD/U_0$. Lee et al. (2020) demonstrated that this dimensionless frequency is associated with the wake-meandering motion downstream of T_1. Chamorro et al. (2013a) likewise observed a similar number ($St = 0.28$) for a standalone horizontal axis tidal turbine with $D = 0.5$ m having the same rotor design as the present turbine. As shown in Fig. 10, the peak of $St = 0.27$, observed upstream of T_2, continues to exist downstream with the same frequency. This implies that the wake-meandering motion initiated upstream of T_2 not only persists downstream of T_2 but also maintains the original frequency. In conclusion, the presence of the second turbine does not affect the frequency of the wake-meandering motion.

At $x'/D = 0.5$, sharp spectral peaks are observed at the rotational frequency of the blade ($f_{blade} \approx 6.4$ Hz) and rotor ($f_{blade}/3 \approx 2.1$ Hz), which are the signatures of the spiral tip vortices around the wake. However, they are observed only up to $x'/D = 1.2$, indicating that the vortices break up downstream of this location.

Downstream of $x'/D = 1.2$ the power spectral density curves at different locations are remarkably similar for $s = 5D$ and $7D$. This shows that the spectral characteristics of the turbulence for $x'/D > 1.2$ are independent of the turbine spacing.

3.4. Integral scale

Although the power spectral density investigated in Section 3.3 provides information about the distributions of the turbulence energy at different scales, the integral scale of turbulence can provide a quantitative measure of the temporal and length scales of turbulent flow structures. The integral time scale of the streamwise velocity component is defined as

$$I_T = \int_0^\infty R_u(s)ds, \tag{1}$$

where R_u is the autocorrelation function for the streamwise velocity fluctuation, $u'(t)$ (t : time), and is given as follows:

$$R_u(s) = \frac{\langle u'(t)u'(t+s)\rangle}{\langle u'(t)^2\rangle}. \tag{2}$$

Using the Taylor's frozen turbulence hypothesis, the integral length scale can be defined as the product of the local mean streamwise velocity $\langle u(t)\rangle$ and the integral time scale (I_T) as given below:

$$I_L = \langle u\rangle I_T. \tag{3}$$

In Fig. 11, the axial profiles of the integral length scales for the heights $z' = 0$ (hub height) and $0.5D$ (top tip height) are plotted. Additionally, the profiles of the single turbine case (dashed lines) are shown for comparison.

In the single turbine case, the integral length scale decreases almost by one order of magnitude as the flow passes T_1. This drop is likely to be associated with the small-scale turbulence generated near the blade tip (tip vortices) and hub locations (hub vortex). As the flow moves away from T_1, the integral scale gradually converges to an approximately constant value of $0.3D$, which should be associated with the large-scale wake-meandering motion.

The profiles in the wake of T_2 for the $s = 5D$ and $7D$ cases show some differences compared with T_1. First, at the top tip, the integral length scale drops only slightly across the location of T_2 ($x' = 0$). This may be due to the high turbulence levels that contribute to the breakdown of the small-scale turbulent flow structures generated by the tip vortices of T_2. Second, at the hub height, the integral scale drop across T_2 is less significant than that observed for T_1, owing to the absence of the core layer's hub vortex structure in the near wake of T_2.

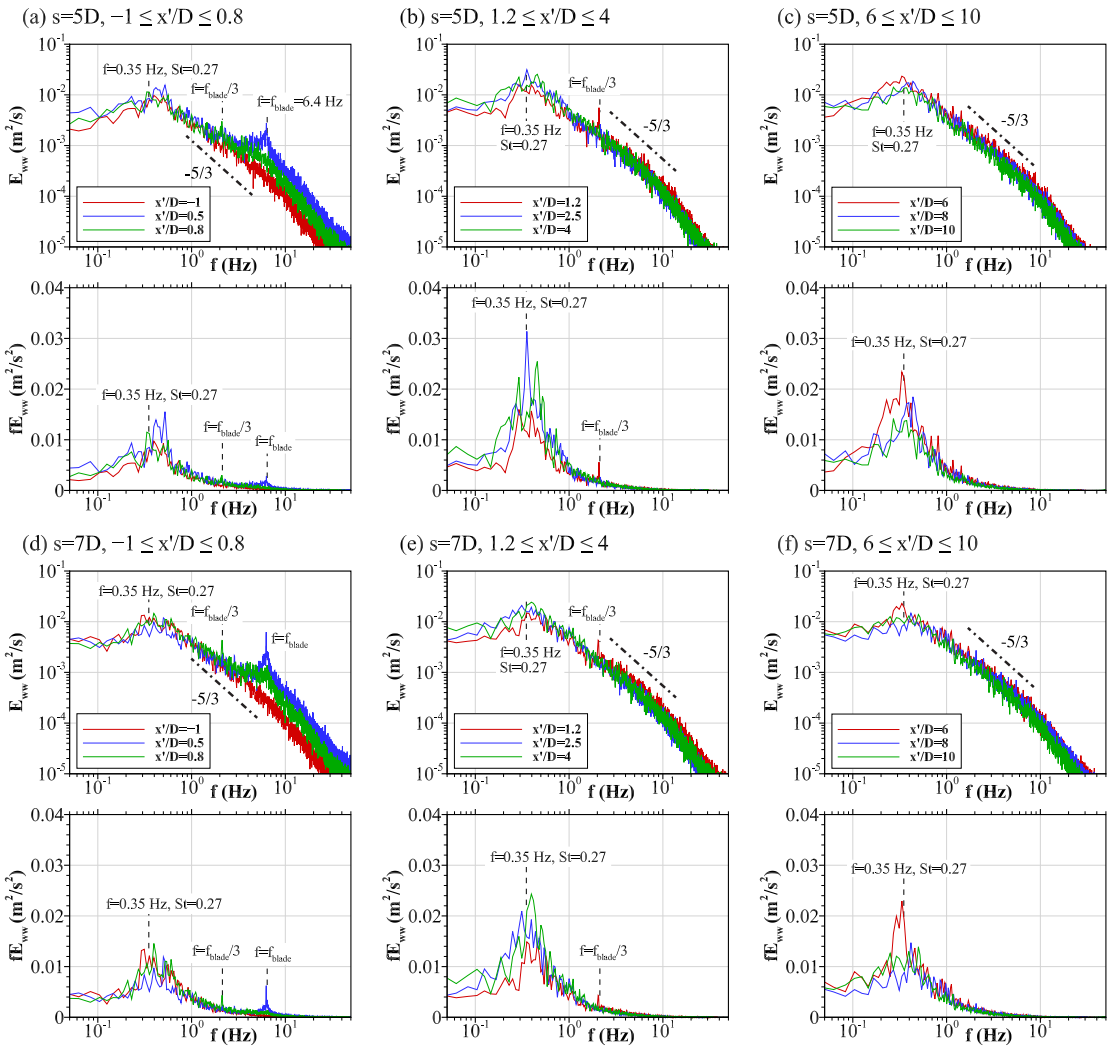

Fig. 10. Velocity spectra for the vertical velocity fluctuations.

In the far-wake region, the integral length scales gradually converge to a value of approximately $0.3D$, similar to that observed in the wake of T_1. The similar integral length scales in the far wakes of T_1 and T_2 are evidence that the characteristic length of the large-scale flow motion, owing to the wake meandering, remains the same downstream of T_2.

A comparison of the integral scales downstream of T_2 between the $s = 5D$ and $7D$ cases is shown in Fig. 11(c). Upon observation, the integral scales are remarkably similar for the two cases at both the hub ($z' = 0$) and the top tip ($z' = 0.5D$) heights. This confirms that, in addition to the flow field contours and velocity spectra, the integral scales in the wake of T_2 are independent of the turbine spacing.

4. Conclusion

The velocity measurements showed that the near-wake structure of T_2 was completely different from that of T_1. Specifically, T_1 showed distinct outer, inner, and core layer structures that were not clearly visible for T_2, whereas T_2 showed a remarkably simple wake pattern in which the shear layers spread from the rotor blade tips toward the rotor axis. The distributions of the mean velocity, TKE, and Reynolds stress behind T_2 were found to be quite similar between the $s = 5D$ and $7D$ cases, indicating that the wake structure of T_2 was virtually independent of the turbine spacing.

In the power spectral density plots, the spectral peak at $St = 0.27$ was found both upstream and downstream of T_2. This revealed that the wake meandering initiated by T_1 persisted downstream of T_2 at the same Strouhal number. Additionally, it was shown that from approximately one to ten rotor diameters downstream of T_2, the power spectral density plots were remarkably similar between the $s = 5D$ and $7D$ cases. This indicates that the turbulence characteristics in the wake of T_2 are independent of the turbine spacing. The integral scale profiles were likewise found to be nearly independent of the turbine spacing.

In summary, the mean flow field, turbulent stress field, velocity spectra, and integral length scales in the wake of T_2 are practically independent of the turbine spacing. This is a remarkable discovery, given that the approach velocities upstream of T_2 differed by approximately 20% between the two cases. To clarify this, it was hypothesized that the increased turbulent momentum transfer as a result of the wake meandering by T_1 overshadowed the effect of the approach velocity on T_2. This indicates that the approach turbulence intensity, rather than the approach velocity, could be a key factor that characterizes the wake structures of turbines within a turbine array.

Therefore, it is reasonable to assume that if the third and fourth turbines are installed downstream of T_2 under similar turbulence intensity conditions, they would exhibit similar wake patterns. As the simple wake pattern observed behind T_2 resembled the numerical results using an actuator disk approach, it can be inferred that the flow in a large tidal farm can be numerically simulated using a simple turbine parameterization approach with satisfactory accuracy. This can be confirmed by further studies using numerical simulations or laboratory experiments.

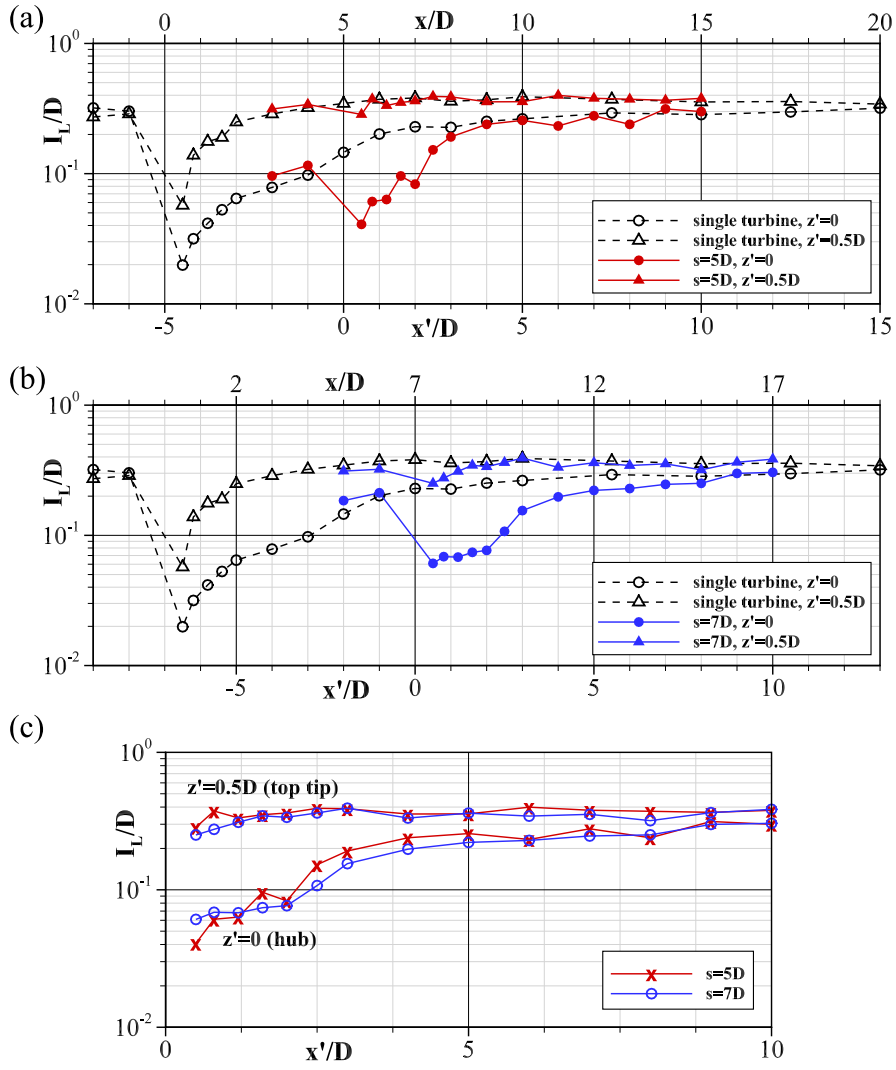

Fig. 11. Axial profiles of the integral length scales.

The limitations of this study are that the torque and power of the turbines were not measured, and that only two spacing conditions were considered. In addition, this study was performed for one specific turbine, and care should be taken when extrapolating the results to other turbines. The effect of turbine geometry on the wake patterns of the second turbine should also be investigated. Further experiments are needed in the future to address these limitations and to provide more comprehensive understanding of turbine wake interactions within tidal arrays.

CRediT authorship contribution statement

SeokKoo Kang: Writing - original draft, Funding acquisition, Supervision. **Youngkyu Kim:** Investigation, Formal analysis. **Jiyong Lee:** Investigation, Formal analysis. **Ali Khosronejad:** Formal analysis. **Xiaolei Yang:** Formal analysis.

Declaration of competing interest

The authors declare that they have no known competing financial interests or personal relationships that could have appeared to influence the work reported in this paper.

Acknowledgments

This research was supported by a grant (21CTAP-C163624-01) from the Infrastructure and Transportation Technology Promotion Research Program funded by the Ministry of Land, Infrastructure and Transport of the Korean government.

References

Abuan, B.E., Howell, R.J., 2019. The performance and hydrodynamics in unsteady flow of a horizontal axis tidal turbine. Renew. Energy 133, 1338–1351.

Apsley, D.D., Stallard, T., Stansby, P.K., 2018. Actuator-line CFD modelling of tidal-stream turbines in arrays. J. Ocean Eng. Mar. Energy 4 (4), 259–271.

Aubrun, S., Loyer, S., Hancock, P., Hayden, P., 2013. Wind turbine wake properties: Comparison between a non-rotating simplified wind turbine model and a rotating model. J. Wind Eng. Ind. Aerodyn. 120, 1–8.

Bahaj, A., Molland, A., Chaplin, J., Batten, W., 2007a. Power and thrust measurements of marine current turbines under various hydrodynamic flow conditions in a cavitation tunnel and a towing tank. Renew. Energy 32 (3), 407–426.

Bahaj, A., Myers, L., Thomson, M., Jorge, N., 2007b. Characterising the wake of horizontal axis marine current turbines. In: Proceedings of the 7th European Wave and Tidal Energy Conference. p. 9.

Batten, W., Bahaj, A., Molland, A., Chaplin, J., 2008. The prediction of the hydrodynamic performance of marine current turbines. Renew. Energy 33 (5), 1085–1096.

Batten, W.M., Harrison, M., Bahaj, A., 2013. Accuracy of the actuator disc-RANS approach for predicting the performance and wake of tidal turbines. Phil. Trans. R. Soc. A 371 (1985), 20120293.
Birjandi, A.H., Bibeau, E.L., Chatoorgoon, V., Kumar, A., 2013. Power measurement of hydrokinetic turbines with free-surface and blockage effect. Ocean Eng. 69, 9–17.
Blackmore, T., Myers, L.E., Bahaj, A.S., 2016. Effects of turbulence on tidal turbines: implications to performance, blade loads, and condition monitoring. Int. J. Mar. Energy 14, 1–26.
Brutto, O.A.L., Thiébot, J., Guillou, S.S., Gualous, H., 2016. A semi-analytic method to optimize tidal farm layouts–Application to the Alderney race (Raz Blanchard), France. Appl. Energy 183, 1168–1180.
Castellani, F., Vignaroli, A., 2013. An application of the actuator disc model for wind turbine wakes calculations. Appl. Energy 101, 432–440.
Chamorro, L., Hill, C., Morton, S., Ellis, C., Arndt, R., Sotiropoulos, F., 2013a. On the interaction between a turbulent open channel flow and an axial-flow turbine. J. Fluid Mech. 716, 658–670.
Chamorro, L.P., Troolin, D.R., Lee, S.-J., Arndt, R., Sotiropoulos, F., 2013b. Three-dimensional flow visualization in the wake of a miniature axial-flow hydrokinetic turbine. Exp. Fluids 54 (2), 1459.
Chawdhary, S., Hill, C., Yang, X., Guala, M., Corren, D., Colby, J., Sotiropoulos, F., 2017. Wake characteristics of a TriFrame of axial-flow hydrokinetic turbines. Renew. Energy 109, 332–345.
Chen, Y., Lin, B., Lin, J., Wang, S., 2015. Effects of stream turbine array configuration on tidal current energy extraction near an island. Comput. Geosci. 77, 20–28.
Chen, Y., Lin, B., Lin, J., Wang, S., 2017. Experimental study of wake structure behind a horizontal axis tidal stream turbine. Appl. Energy 196, 82–96.
Ebdon, T., Allmark, M.J., O'Doherty, D.M., Mason-Jones, A., O'Doherty, T., Germain, G., Gaurier, B., 2021. The impact of turbulence and turbine operating condition on the wakes of tidal turbines. Renew. Energy 165, 96–116.
Fallon, D., Hartnett, M., Olbert, A., Nash, S., 2014. The effects of array configuration on the hydro-environmental impacts of tidal turbines. Renew. Energy 64, 10–25.
Gaurier, B., Carlier, C., Germain, G., Pinon, G., Rivoalen, E., 2020. Three tidal turbines in interaction: An experimental study of turbulence intensity effects on wakes and turbine performance. Renew. Energy 148, 1150–1164.
Gunawan, B., Neary, V.S., Colby, J., 2014. Tidal energy site resource assessment in the East River tidal strait, near Roosevelt Island, New York, New York. Renew. Energy 71, 509–517.
Hill, C., Musa, M., Guala, M., 2016. Interaction between instream axial flow hydrokinetic turbines and uni-directional flow bedforms. Renew. Energy 86, 409–421.
Kang, S., Borazjani, I., Colby, J.A., Sotiropoulos, F., 2012. Numerical simulation of 3D flow past a real-life marine hydrokinetic turbine. Adv. Water Resour. 39, 33–43.
Kang, S., Yang, X., Sotiropoulos, F., 2014. On the onset of wake meandering for an axial flow turbine in a turbulent open channel flow. J. Fluid Mech. 744, 376–403.
Khan, M., Bhuyan, G., Iqbal, M., Quaicoe, J., 2009. Hydrokinetic energy conversion systems and assessment of horizontal and vertical axis turbines for river and tidal applications: A technology status review. Appl. Energy 86 (10), 1823–1835.
Lago, L.I., Ponta, F.L., Chen, L., 2010. Advances and trends in hydrokinetic turbine systems. Energy Sustain. Dev. 14 (4), 287–296.
Laws, N.D., Epps, B.P., 2016. Hydrokinetic energy conversion: Technology, research, and outlook. Renew. Sustain. Energy Rev. 57, 1245–1259.
Lee, J., Kim, Y., Khosronejad, A., Kang, S., 2020. Experimental study of the wake characteristics of an axial flow hydrokinetic turbine at different tip speed ratios. Ocean Eng. 196, 106777.
Lewis, M., Neill, S., Robins, P., Hashemi, M., 2015. Resource assessment for future generations of tidal-stream energy arrays. Energy 83, 403–415.
Maganga, F., Germain, G., King, J., Pinon, G., Rivoalen, E., 2010. Experimental characterisation of flow effects on marine current turbine behaviour and on its wake properties. IET Renew. Power Gener. 4 (6), 498–509.
Morandi, B., Felice, F.D., Costanzo, M., Romano, G., Dhome, D., Allo, J., 2016. Experimental investigation of the near wake of a horizontal axis tidal current turbine. Int. J. Mar. Energy 14, 229–247.
Musa, M., Hill, C., Guala, M., 2019. Interaction between hydrokinetic turbine wakes and sediment dynamics: array performance and geomorphic effects under different siting strategies and sediment transport conditions. Renew. Energy 138, 738–753.
Musa, M., Hill, C., Sotiropoulos, F., Guala, M., 2018. Performance and resilience of hydrokinetic turbine arrays under large migrating fluvial bedforms. Nat. Energy 3 (10), 839–846.
Mycek, P., Gaurier, B., Germain, G., Pinon, G., Rivoalen, E., 2013. Numerical and experimental study of the interaction between two marine current turbines. Int. J. Mar. Energy 1, 70–83.
Mycek, P., Gaurier, B., Germain, G., Pinon, G., Rivoalen, E., 2014a. Experimental study of the turbulence intensity effects on marine current turbines behaviour. Part I: One single turbine. Renew. Energy 66, 729–746.
Mycek, P., Gaurier, B., Germain, G., Pinon, G., Rivoalen, E., 2014b. Experimental study of the turbulence intensity effects on marine current turbines behaviour. Part II: Two interacting turbines. Renew. Energy 68, 876–892.
Myers, L., Bahaj, A., 2007. Wake studies of a 1/30th scale horizontal axis marine current turbine. Ocean Eng. 34 (5), 758–762.
Neary, V.S., Gunawan, B., Hill, C., Chamorro, L.P., 2013. Near and far field flow disturbances induced by model hydrokinetic turbine: ADV and ADP comparison. Renew. Energy 60, 1–6.
Nuernberg, M., Tao, L., 2018a. Experimental study of wake characteristics in tidal turbine arrays. Renew. Energy 127, 168–181.
Nuernberg, M., Tao, L., 2018b. Three dimensional tidal turbine array simulations using openfoam with dynamic mesh. Ocean Eng. 147, 629–646.
Ouro, P., Harrold, M., Stoesser, T., Bromley, P., 2017. Hydrodynamic loadings on a horizontal axis tidal turbine prototype. J. Fluids Struct. 71, 78–95.
Rourke, F.O., Boyle, F., Reynolds, A., 2010. Tidal energy update 2009. Appl. Energy 87 (2), 398–409.
Sandoval, J., Soto-Rivas, K., Gotelli, C., Escauriaza, C., 2021. Modeling the wake dynamics of a marine hydrokinetic turbine using different actuator representations. Ocean Eng. 222, 108584.
Sørensen, J.N., Mikkelsen, R.F., Henningson, D.S., Ivanell, S., Sarmast, S., Andersen, S.J., 2015. Simulation of wind turbine wakes using the actuator line technique. Phil. Trans. R. Soc. A 373 (2035), 20140071.
Stallard, T., Collings, R., Feng, T., Whelan, J., 2013. Interactions between tidal turbine wakes: experimental study of a group of three-bladed rotors. Phil. Trans. R. Soc. A 371 (1985), 20120159.
Stallard, T., Feng, T., Stansby, P., 2015. Experimental study of the mean wake of a tidal stream rotor in a shallow turbulent flow. J. Fluids Struct. 54, 235–246.
Stansby, P., Stallard, T., 2016. Fast optimisation of tidal stream turbine positions for power generation in small arrays with low blockage based on superposition of self-similar far-wake velocity deficit profiles. Renew. Energy 92, 366–375.
Wang, S.-Q., Zhang, Y., Xie, Y.-y., Xu, G., Liu, K., Zheng, Y., 2021. The effects of surge motion on hydrodynamics characteristics of horizontal-axis tidal current turbine under free surface condition. Renew. Energy 170, 773–784.
Xie, T., Wang, T., He, Q., Diallo, D., Claramunt, C., 2020. A review of current issues of marine current turbine blade fault detection. Ocean Eng. 218, 108194.
Yang, X., Kang, S., Sotiropoulos, F., 2012. Computational study and modeling of turbine spacing effects in infinite aligned wind farms. Phys. Fluids 24 (11), 115107.
Yang, X., Sotiropoulos, F., 2018. A new class of actuator surface models for wind turbines. Wind Energy 21 (5), 285–302.
Yuce, M.I., Muratoglu, A., 2015. Hydrokinetic energy conversion systems: A technology status review. Renew. Sustain. Energy Rev. 43, 72–82.
Zhou, Z., Scuiller, F., Charpentier, J.F., Benbouzid, M., Tang, T., 2014. An up-to-date review of large marine tidal current turbine technologies. In: 2014 International Power Electronics and Application Conference and Exposition. IEEE, pp. 480–484.
Zhu, Q., Yan, J., 2021. A moving-domain CFD solver in FEniCS with applications to tidal turbine simulations in turbulent flows. Comput. Math. Appl. 81, 532–546.